Intermetallics 129 (2021) 107052

Contents lists available at ScienceDirect

Intermetallics

journal homepage: http://www.elsevier.com/locate/intermet

Synthesis, crystal chemistry, and magnetic properties of $Ce_{3-x}RhGa_{10+3x}$ (x = 0.36): A new member of the $[BaAl_4]_m[CaF_2]_n[AlB_2]_p$ homologous series

Sergey Nesterenko [a], Anna Tursina [a,*], Dariusz Kaczorowski [b,c]

[a] Department of Chemistry, Lomonosov Moscow State University, 119991, Moscow, Russia
[b] Institute of Low Temperature and Structure Research, Polish Academy of Sciences, Okólna 2, 50-422, Wrocław, Poland
[c] Institute of Molecular Physics, Polish Academy of Sciences, Smoluchowskiego 17, 60-179, Poznań, Poland

ARTICLE INFO

Keywords:
Intermetallics
Crystal chemistry
Electrical properties
Magnetic properties
Site occupancy

ABSTRACT

$Ce_{3-x}RhGa_{10+3x}$ (x = 0.36) is a new member of the linear intergrowth structure series built up from segments of the $BaAl_4$, AlB_2 and CaF_2 structure types. The compound crystallizes with a disordered variant of the Pr_3NiGa_{10} type structure. Unlike the prototype, $Ce_{3-x}RhGa_{10+3x}$ exhibits notable deficiency in rare-earth content, accompanied with significant excess of Ga atoms, corresponding to additional Ga environment of one of the Ce atoms. The novel compound is a Curie-Weiss paramagnet and orders antiferromagnetically at low temperatures. The electrical transport in $Ce_{3-x}RhGa_{10+3x}$ has a metallic character, and bears contributions due to crystalline electric field, Kondo and magnetic exchange interactions.

1. Introduction

Ternary cerium gallides with *d*-electron transition metals exhibit a wide range of interesting crystal structure related physical properties, like complex magnetic orderings, heavy fermion phenomena or non-Fermi liquid behavior [1,2]. In addition, some of these compounds have been recognized as good candidates for potential applications, e.g., as magnetocaloric materials or hydrogenation catalysts [1].

Especially interesting appear ternaries bearing 4*d* or 5*d* element and large Ga content. The compounds $CePdGa_6$ [3,4] and Ce_2PdGa_{10} [5] are antiferromagnetic heavy fermion systems [4–6], while the alloy series $CePd_xGa_{4-x}$ is ferromagnetic at low temperatures [6,7]. In turn, strong electronic correlations in $CePdGa_3$ [8], $CePd_3Ga_8$ [9] and $Ce_{1.33}Pt_4Ga_{10}$ [10] are not accompanied with any magnetic phase transition down to 2 K, and all three materials were characterized as paramagnetic Kondo lattices. Heavy fermion behavior was reported also for $Ce_2Pt_6Ga_{15}$, however this compound has an electronic ground state of non-Fermi liquid character [11]. In contrast, rather weak electronic correlations were observed in strongly anisotropic antiferromagnet Ce_2PdGa_{12} that exhibits two subsequent magnetic phase transitions at low temperatures and intriguing metamagnetic features [4,12]. Similar magnetic properties were reported for the isostructural phases Ce_2RhGa_{12} [13], Ce_2PtGa_{12} [14] and Ce_2IrGa_{12} [15].

Even though no unconventional superconductor has been identified as yet amidst the Ce-bearing ternary gallides, over nearly two decades, search for the first representative has been continuously stimulated by the seminal discovery of the heavy-fermion superconductor $PuCoGa_5$ having an extremely high critical temperature of 18 K [16]. Recently, another motivation for such research arose due to the recognition of gallium clusters as a favorable structural motif for superconductivity emerging in endohedral phases based on transition element or/and rare earth atoms [17].

In the course of our on-going study on the phase equilibria in the ternary Ce–Rh-Ga system, we have recently established the formation of previously unknown ternary compound with a limited range of composition. Our preliminary characterization of this phase [18], indicated the stoichiometry $Ce_{3-x}RhGa_{10+3x}$ with x = 0.36, and suggested an orthorhombic crystal structure of the Pr_3NiGa_{10} type. In this paper, we report on our exhaustive structural investigation of the novel Ga-rich compound as well as our studies on its low-temperature physical properties.

2. Experimental

A polycrystalline sample of Ce18Rh6.8Ga75.2 composition was prepared by direct reaction of the pure elements (Ce 99.85%, Rh 99.99%, Ga 99.999%) in an Edmund Bühler MAM-1 compact arc furnace on a water-cooled copper hearth under protective argon

* Corresponding author.
E-mail address: anna.i.tursina@gmail.com (A. Tursina).

https://doi.org/10.1016/j.intermet.2020.107052
Received 11 October 2020; Received in revised form 17 November 2020; Accepted 22 November 2020
Available online 28 November 2020

Table 1
Crystal data and refinement parameters for $Ce_{3-x}RhGa_{10+3x}$ (x = 0.36).

Space group	*Pmmm* (No 47)
a (Å)	4.2952(14), 4.2981(7)*
b (Å)	4.3126(15), 4.3175(8)*
c (Å)	15.545(3), 15.5573(19)*
Cell volume (Å^3)	287.94 (15)
Z	1
D_{calc} (g*cm^{-3})	7.069
Absorbtion coefficient (mm^{-1})	36.318
Radiation (Å)	MoK$_\alpha$, 0.71073
Index range	$-7 \le h \le 1$, $-3 \le k \le 6$, $0 \le l \le 23$
Θ range	1.310°–36.931°
Number of measured reflections	722
Number of reflections with I ≥ 2σI	549
Number of refined parameters	45
R_F, R_W	0.0553, 0.1514
Goodness of fit	1.065

* – powder data.

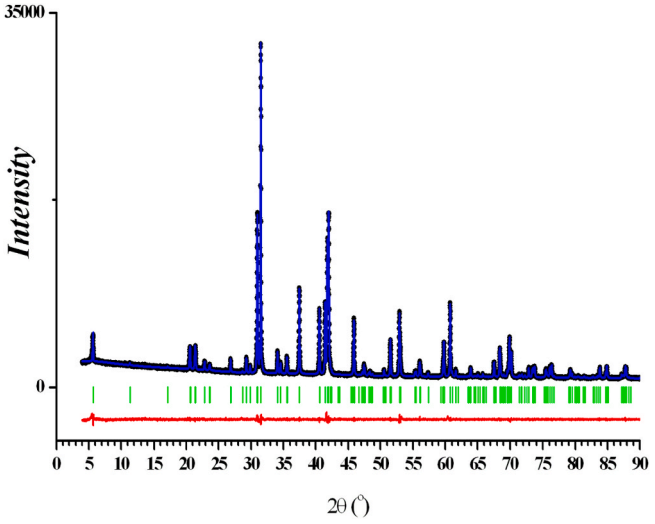

Fig. 1. Rietveld refined powder XRD pattern of the $Ce_{3-x}RhGa_{10+3x}$ sample showing the experimental (black dots), calculated (blue solid line) and difference (red) profiles (χ^2 = 1.550, R_p = 0.0220, R_{wp} = 0.0307, R_{exp} = 0.0240, R_{Bragg} = 0.0801). The green vertical bars denote the calculated positions of the Bragg peaks.

Table 2
Fractional atomic coordinates and equivalent displacement parameters (U_{eq}) refined for $Ce_{3-x}RhGa_{10+3x}$ (x = 0.36).

Atom	Site	Occupancy	x/*a*	y/*b*	z/*c*	U_{eq} (Å^2)
Ce1	1*a*	0.638 (9)	0	0	0	0.0067(7)
Ce2	2*r*	1	0	0.5	0.25586(8)	0.0052(3)
Rh	1*g*	1	0	0.5	0.5	0.0049(4)
Ga1	2*t*	1	0.5	0.5	0.08094(19)	0.0286(8)
Ga2	2*t*	1	0.5	0.5	0.41401(16)	0.0066(5)
Ga3	2*s*	1	0.5	0	0.15838(19)	0.0173(6)
Ga4	2*s*	1	0.5	0	0.31486(17)	0.0064(4)
Ga5	2*q*	1	0	0	0.41424(16)	0.0068(5)
Ga6	2*q*	0.145(13)	0	0	0.0890(13)	0.018(5)
Ga7	4*u*	0.127(7)	0	0.277(5)	0.0583(16)	0.040(6)

atmosphere. To account for relatively high volatility of liquid gallium at very high temperatures an excess of 0.5 mass% of this element was added beforehand. The process was repeated at least three times to ensure uniformity and homogeneity. Subsequently, the melted ingot was annealed in an evacuated silica tube at 700 °C for 750 h.

The chemical composition of the annealed sample was checked by energy dispersive X-ray (EDX) analysis performed using a Carl Zeiss LEO EVO 50XVP scanning electron microscope equipped with an EDX-spectrometer INCA Energy 450 (Oxford Instruments). Its crystal structure was examined by powder X-ray diffraction (XRD) employing a STOE STADI P transmission diffractometer with CuK$_{\alpha1}$-radiation (λ = 1.54056 Å), equipped with a Ge (111) monochromator and a linear position-sensitive detector. The measurement was done within an angle range 4° ≤ 2θ ≤ 90.09° with a scan step of 0.01°. The powder XRD data were analyzed using the MRIA program [19].

Single crystals useful for XRD data collection were isolated from crushed as-cast polycrystalline ingot. The experiment was performed using a CAD4 Enraf-Nonius diffractometer (MoK$_\alpha$-radiation, ω/θ-scan). The structure was solved by direct methods and refined by full-matrix least-square procedures (SHELXL-2018/3) [20]. All of the sites were refined with anisotropic displacement parameters. In the final steps of structure refinement, additional peaks of electron density forming a distorted hexagon around Ce1 position were observed on the difference Fourier maps. These peaks were attributed to the two partially occupied Ga6 (2*q*) and Ga7 (4*u*) sites. Refined occupancy of the Ce1 position was approximately equal to 0.67. Excluding unrealistic short Ce–Ga and Ga–Ga interatomic distances, it was found that one third of Ce1 is replaced by Ga6-Ga7-Ga7 triangle. Therefore, in the final cycles of refinement, appropriate constraints were applied. Atomic parameters were standardized using the program STRUCTURE TIDY [21]. Unit cell, polyhedra and structure details were visualized using the program DIAMOND [22]. The refined crystal structure of $Ce_{3-x}RhGa_{10+3x}$ was deposited to the joint CCDC/FIZ Karlsruhe database via www.ccdc.cam.ac.uk with the reference number 1977875. Details on the performed XRD experiment and the structure refinements are gathered in Table 1.

Low-temperature physical measurements were performed on appropriately shaped polycrystalline specimens. Magnetic behavior was studied in the temperature range 1.72–300 K and in magnetic fields up to 5 T using a Quantum Design MPMS-5 SQUID magnetometer. Heat capacity and electrical transport measurements were carried out in the temperature interval 2–300 K and in magnetic fields up to 9 T employing a Quantum Design PPMS-9 platform. The specific heat was measured using a relaxation method fixing the specimen using Apiezon N grease. The electrical resistivity was measured employing a standard ac four-point technique. The electrical leads were mounted to the specimen using silver epoxy paste.

3. Results and discussion

3.1. Polycrystalline sample characterization

The powder XRD pattern of the prepared polycrystalline sample of Ce18Rh6.8Ga75.2 is presented in Fig. 1. The Rietveld analysis indicated that the sample was single-phase, and has an orthorhombic unit cell. The calculated lattice parameters were fairly close to those obtained from the single-crystal XRD data (see Table 1).

The EDX study revealed that aside from the majority phase having the composition Ce18.3Rh6.8Ga74.9, the Ce18Rh6.8Ga75.2 sample contains tiny traces of a foreign phase with the composition Ce12.8Rh20.3Ga66.9 that can be identified as the ternary compound $Ce_2Rh_3Ga_9$ [23].

3.2. Crystal structure

The single-crystal XRD experiment showed that the crystal structure of $Ce_{3-x}RhGa_{10+3x}$ has the orthorhombic Pr_3NiGa_{10}-type structure [24] with the space group *Pmmm* (No 47) and the lattice parameters: *a* = 4.2952(14) Å, *b* = 4.3126(15) Å, *c* = 15.545(3) Å and V = 287.94(15) Å^3. In the crystallographic unit cell there are as many as ten nonequivalent atomic sites, seven of which are fully occupied and three (Ce1, Ga6, and Ga7) have partial occupancies. The refined atomic and

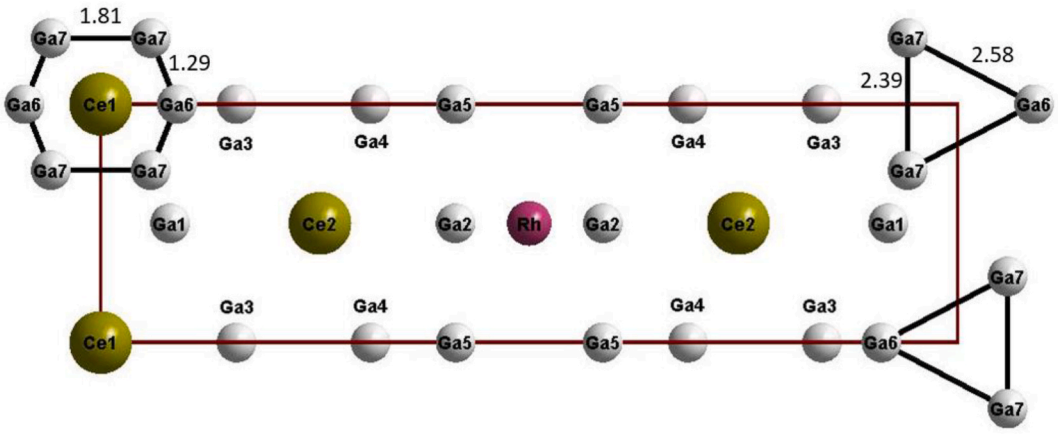

Fig. 2. Projection of $Ce_{3-x}RhGa_{10+3x}$ crystal structure along the *a*-axis. Cerium, rhodium, and gallium atoms are drawn as green, red and grey spheres, respectively. Gallium hexagon and triangles are emphasized.

Table 3
Interatomic distances (*d*) in $Ce_{3-x}RhGa_{10+3x}$ (x = 0.36).

Atom	To atom	*d*, Å	Atom	To atom	*d*, Å
Ce1	4 Ga3	3.267(2)	Ga4	Ga3	2.433(4)
	8 Ga1	3.2931(13)		2 Ga5	2.645(2)
Ce2	4 Ga4	3.1785(11)		2 Ga2	2.651(2)
	2 Ga2	3.264(2)		4 Ce2	3.1785(11)
	2 Ga5	3.273(2)	Ga5	2 R h	2.5351(15)
	4 Ga3	3.3997(16)		2 Ga4	2.645(2)
	2 Ga1	3.465(3)		Ga5	2.666(5)
Rh	4 Ga2	2.5296(15)		4 Ga2	3.0433(7)
	4 Ga5	2.5351(15)		2 Ce2	3.273(2)
Ga1	2 Ga3	2.470(2)	Ga6	2 Ga3	2.403(9)
	Ga1	2.516(6)		2 Ga7	2.58(3)
	4 Ce1	3.2931(13)		Ga6	2.77(4)
	2 Ce2	3.465(3)		4 Ga1	3.0459(11)
Ga2	2 R h	2.5296(15)		2 Ga7	3.15(2)
	2 Ga4	2.651(2)		2 Ce2	3.22(2)
	4Ga5	3.0433(7)	Ga7	2 Ga1	2.379(9)
	Ga2	2.673(5)		Ga7	2.39(4)
	2 Ce2	3.264(2)		Ga6	2.58(3)
Ga3	Ga4	2.433(4)		Ga7	2.64(5)
	2 Ga1	2.470(2)		2 Ga3	2.909(18)
	2 Ce1	3.267(2)		Ga7	3.00(4)
	4 Ce2	3.3997(16)		Ga6	3.15(2)
				2 Ga1	3.20(2)
				Ce2	3.22(2)

isotropic equivalent displacement parameters are given in Table 2.

Unlike in the prototype structure, in the $Ce_{3-x}RhGa_{10+3x}$ unit cell, one of the RE atoms sites, namely the Ce1 site, is occupied only partially. Moreover, some deficiency occurs at two additional Ga atoms positions, viz. the Ga6 and Ga7 sites. It should be noted that the Ce1 atoms and the Ga6 and Ga7 atoms cannot reside concurrently in the unit cell, as this gives rise to too short distances *d*(Ce1−Ga6) = 1.38 Å and *d*(Ce1−Ga7) = 1.50 Å (see Fig. 2). The calculated occupancy values of Ce1, Ga6, and Ga7 hint at statistical substitution of these two Ga atoms for the Ce atom. In turn, in the hexagon built of two Ga6 and four Ga7 atoms surrounding Ce1, those Ga positions cannot be fully occupied because it would lead to unrealistically short contacts Ga6−Ga7 = 1.29 Å and Ga7−Ga7 = 1.81 Å. The occupancy factors obtained for Ga6 and Ga7 indicate that at the most half of the hexagon positions are occupied. This finding implies that the Ga atoms can be distributed over alternating sites located at distances *d*(Ga6−Ga7) = 2.58 (3) Å and *d*(Ga7−Ga7) = 2.39 (4) Å (see Table 3), which are close to ordinary Ga–Ga separation. Thus, in the crystal structure of $Ce_{3-x}RhGa_{10+3x}$, the Ce1 atoms are statistically substituted by the Ga6-Ga7-Ga7 triangles with two possible orientations in the unit cell, as visualized in Fig. 2. Similar substitutional phenomena of alkaline earth or rare-earth atoms by Ga_3 triangular units was reported to occur in several binary and ternary gallides [25–28].

As shown in Fig. 3, the Ce1 atom is coordinated by twelve Ga atoms, which form an almost regular hexagonal prism. The interatomic distances *d*(Ce1−Ga1) and *d*(Ce1−Ga3) are 3.2931(13) Å and 3.267(2) Å, respectively. The environment of the Ce2 atom is built of four Ga4 atoms at a distance of 3.1785(11) Å, four Ga3 at 3.3997(16) Å, two Ga2 atoms at 3.264(2) Å, and two Ga1 atoms at 3.465(3) Å, forming a severely distorted hexagonal prism that includes two additional face-capping Ga5 atoms located at a distance of 3.273(2) Å. In both Ce1 and Ce2 polyhedra, all the Ce−ligand distances are significantly larger than the respective sums of the single-bond covalent radii of the elements [29].

The coordination polyhedron of the Rh atom is a tetragonal prism made of four Ga2 and four Ga5 atoms (see Fig. 3). The length of the Rh−Ga2 and Rh−Ga5 bonds are 2.5296(15) Å and 2.5351(15) Å, respectively. The Ga1, Ga3 and Ga4 atoms are surrounded by tricapped trigonal prisms of composition Ga1[Ce_6Ga_3], Ga3[Ce_6Ga_3], and Ga4 [Ce_4Ga_5], respectively (Fig. 3). The Ga2 and Ga5 atoms are located in the center of almost identical tricapped tetragonal prisms Ga [$Ce_2Rh_2Ga_7$] (Fig. 3). In turn, the Ga6 and Ga7 atoms are coordinated to two Ce2 atoms and twelve gallium atoms. As can be inferred from Table 3, all the Ga–Ga distances are comparable to the sum of single-bond covalent radii (2.50 Å) [29], and in some cases they are shorter than the average Ga–Ga distance found in metallic gallium (1 × 2.44 and 6 × 2.70 Å) [30]. Based on the observed features, the structure of $Ce_{3-x}RhGa_{10+3x}$ can be presented as a packing of condensed Ce1[Ga_{12}], Ce2[Ga_{14}] and Rh[Ga_8] polyhedra (see Fig. 4), and hence the novel compound can be assigned to the endohedral gallide cluster materials.

As depicted in Fig. 5, the crystal structure of $Ce_{3-x}RhGa_{10+3x}$ can also be described in terms of linear inhomogeneous intergrowth of topologically related fragments, viz., $BaAl_4$-, AlB_2- and CaF_2-type slabs [31–33] stacked along the crystallographic *c*-direction. The $BaAl_4$ slab consists of the Ga4-centered tetragonal antiprisms situated between two networks of the Ce2 and Ga2-Ga5 atoms, which form associated square nets. Within the AlB_2 fragments, the Ga3 atoms are located in the center of the face-sharing trigonal prisms formed by the Ce1 and Ce2 atoms. In turn, the CaF_2-type slabs consist of the face-connected tetragonal prisms formed by eight Ga atoms, half of which being centered by the Rh atoms. The neighboring $BaAl_4$ blocks share a common square face of the Ga2 and Ga5 atoms with the empty tetragonal prisms in the CaF_2-type slab. Consequently, $Ce_{3-x}RhGa_{10+3x}$ can be considered as a new member of a structural series of compounds with the general formula $R_{0.5m+p}X_{2m+3n+2p}$, for the first time reported by Grin et al. [24], where R and X denote elements with markedly different atomic radii ($r_R > r_X$), and indexes *m*, *n*, *p* designate the numbers of consecutive intergrowth $BaAl_4$-, CaF_2- and AlB_2-type slabs, respectively.

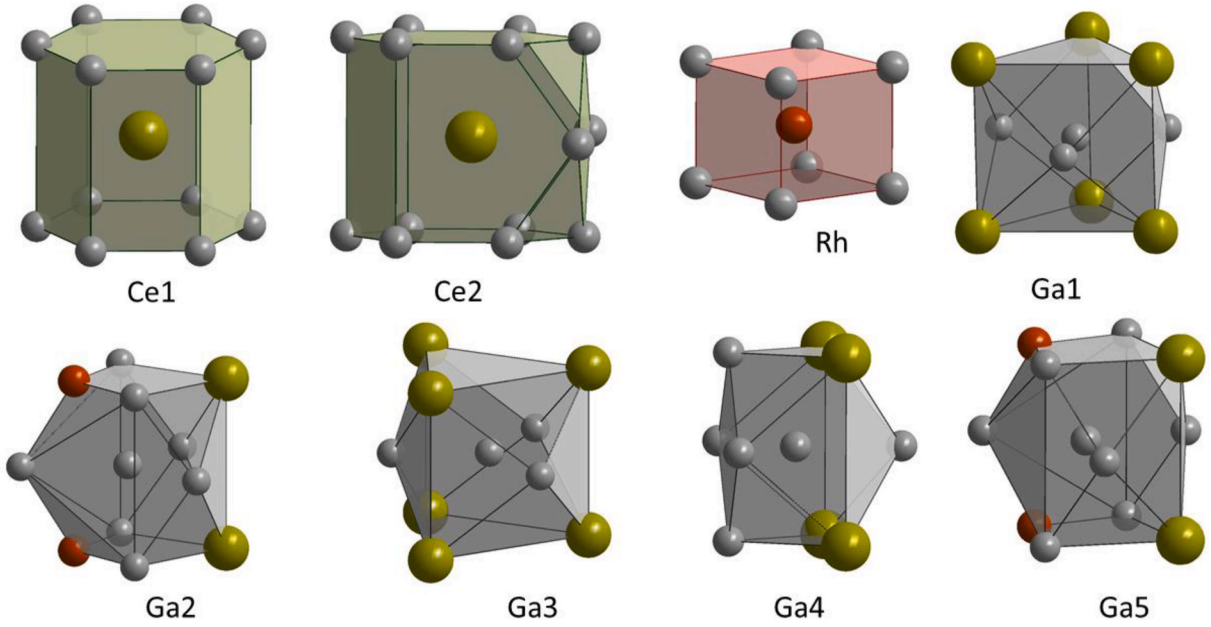

Fig. 3. The local coordination of atoms in $Ce_{3-x}RhGa_{10+3x}$. Ce atoms are green, Rh atoms are red, and Ga atoms are grey. Ga6 and Ga7 atoms with low occupancies are omitted.

In Fig. 5, the crystal structure of $Ce_{3-x}RhGa_{10+3x}$ is compared with the structures of $U_2Ni_2Si_7$, $EuMg_3Ge_3$, and $Th_2Au_3Al_4Si_2$, which also consist of fragments of the $BaAl_4$-, CaF_2- and AlB_2-types in different ratios and/or connection sequences [34–36]. It should be pointed out that in $Ce_{3-x}RhGa_{10+3x}$, two types of layers that act as building blocks for the structure do not have any counterparts among corresponding binary compounds of the CaF_2- and $BaAl_4$- type, respectively, while the AlB_2--type compound $CeGa_2$ does exist.

Finally, it should be noted that the ternary phase $Ce_{3-x}RhGa_{10+3x}$ can be regarded as an interstitial derivative of hypothetical "$Ce_{3-x}Ga_{8+3x}$" binary gallide of the $Sr_{3-x}Ga_{8+3x}$-type (space group *Immm*, Z = 2) [25]. The unit cell of the compound $Sr_{3-x}Ga_{8+3x}$ has the lattice parameters: a = 4.3958(9) Å, b = 4.5298(6) Å, c = 26.002(4) Å [25]. In $Ce_{3-x}RhGa_{10+3x}$, the CaF_2-type slab is defined by the Ga2 and Ga5 atoms, which form tetragonal prims with a thickness of 2.67 Å that corresponds to the interatomic distances d(Ga2−Ga2) and d(Ga5−Ga5) of 2.673(5) Å and 2.666(5) Å, respectively. Due to addition of one $RhGa_2$ slab (CaF_2-type) with a thickness of 2.67 Å per each $Sr_{3-x}Ga_{8+3x}$ formula unit, the c parameter of the unit cell expands from 26.00 Å in $Sr_{3-x}Ga_{8+3x}$ to 31.34 Å in "$Sr_{3-x}RhGa_{10+3x}$", which would correspond to 15.67 Å, if Z = 1. The later value coincides fairly well with the actually observed c parameter of $Ce_{3-x}RhGa_{10+3x}$ (c = 15.545(3) Å).

3.3. Physical properties

Fig. 6 presents the magnetic behavior of $Ce_{3-x}RhGa_{10+3x}$ (x = 0.36). Below room temperature, the inverse molar magnetic susceptibility is a linear function of temperature, expected for a Curie-Weiss (CW) paramagnet. The effective magnetic moment and the paramagnetic Curie temperature derived from the CW formula $\chi(T) = C/(T - \theta_p)$ amount to $\mu_{eff} = \sqrt{8C} = 3.88\ \mu_B$ (C stands for the Curie constant) and $\theta_p = -4.0$ (1) K, respectively. The value of μ_{eff} calculated per Ce atom corresponds to 2.53 (1) μ_B that is almost equal to the theoretical Russell-Saunders value for trivalent Ce ion (2.54 μ_B). The negative value of θ_p signals antiferromagnetic (AFM) exchange correlations.

Below about 30 K, $\chi(T)$ slightly deviates from the CW law, likely due to crystalline electric field (CEF) effect and magnetic exchange interaction. As displayed in the upper inset to Fig. 6, a small maximum in $\chi(T)$ occurs at 3.6 K, marking an onset of AFM state. At the lowest temperatures covered, $\chi(T)$ shows an upturn that might indicate complex spin structure or occurrence of another magnetic transition below 1.72 K.

The AFM nature of $Ce_{3-x}RhGa_{10+3x}$ at the later temperature was corroborated by measuring the magnetization versus magnetic field. The obtained isotherm (see the lower inset to Fig. 6) is initially linear in weak fields, and undergoes an inflection near 0.8 T that signals a metamagnetic transition. In the strongest fields examined, σ(H) exhibits a faint tendency towards saturation. In the terminal field of 5 T, the magnetization attains a value of 10.56 (3) emu/g that corresponds to the magnetic moment m_{5T} = 1.0 (1) μ_B per Ce atom in the alloy $Ce_{3-x}RhGa_{10+3x}$ with x = 0.36. The magnitude of m_{5T} is distinctly smaller than the magnetic moment of free Ce3+ ion (2.14 μ_B), and this reduction can be attributed mostly to the CEF effect.

Bulk character of the AFM phase transition in $Ce_{3-x}RhGa_{10+3x}$ was further confirmed by the heat capacity data. As clearly seen in the inset to Fig. 7, the specific heat exhibits at low temperatures a mean-field type anomaly at T_N = 3.6 K, in concert with $\chi(T)$. In the paramagnetic region, C(T) has a regular sigmoid-like shape, which results mostly from the temperature dependence of the phonon contribution. Near 300 K, the specific heat saturates at a value of about 350 J/(mol K) that is fairly close to the Dulong-Petit limit for $Ce_{3-x}RhGa_{10+3x}$ with x = 0.36 (3nR = 367.2 J/(mol K); n = 14.72 is the number of atoms per formula unit, and R stands for the universal gas constant).

As depicted in Fig. 8, in the temperature range 10–20 K, the C/T ratio is a linear function of T^2. From the Debye formula $C(T) = \gamma T + \beta T^3$, one can derive the Sommerfeld coefficient γ = 388.8 (4) mJ/(mol K^2) and the phonon coefficient β = 2.408 (8) mJ/(mol K^4). The latter value

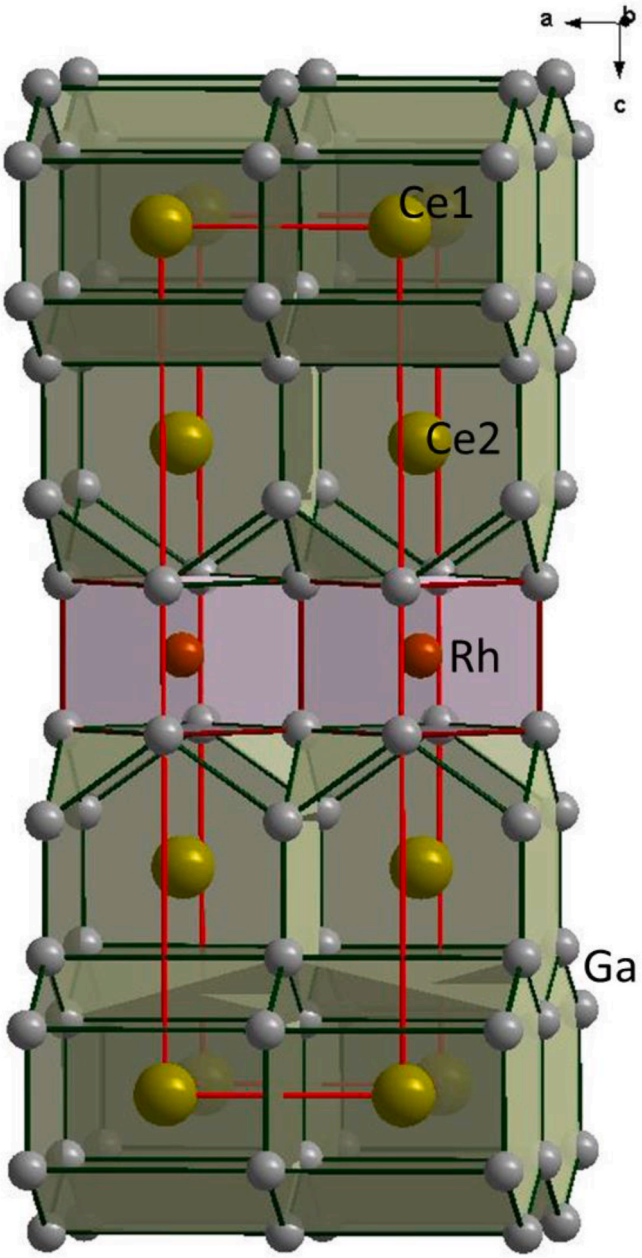

Fig. 4. Polyhedral representation of the $Ce_{3-x}RhGa_{10+3x}$ structure assigned to the endohedral gallide cluster materials.

implies the Debye temperature $\Theta_D = 228$ K, computed from the relationship $\Theta_D = [12\,R\pi^4 n/(5\beta)]^{1/3}$. It should be noted however that the so-obtained value of Θ_D should be regarded merely as a rough estimate because the temperature region from which it was derived does not comply with general validity condition ($T < \Theta_D/50$) of the approach applied.

Fig. 9 presents the temperature dependence of the electrical resistivity of $Ce_{3-x}RhGa_{10+3x}$. At 300 K, the resistivity equals 93 μΩcm, and with decreasing temperature, it decreases in a metallic manner down to 48 μΩcm at 2 K. The latter value is rather large as for a Ce-based intermetallic material. This feature can be attributed to structural disorder in the crystal structure of $Ce_{3-x}RhGa_{10+3x}$, where one Ce site and two Ge sites show partial occupancies. Near 50 K, ρ(T) exhibits a broad hump that is likely a combined effect of the CEF and Kondo interactions.

The AFM phase transition at $T_N = 3.6$ K manifests itself as a kink in ρ(T) that brings about a sharp maximum in the temperature derivative of the ρ(T) function (see the inset to Fig. 9). Below about 3 K, dρ/dT shows a sharp upturn, which may be considered as another hint at complex AFM spin structure in $Ce_{3-x}RhGa_{10+3x}$, anticipated from the magnetic susceptibility data.

Upon applying magnetic field, the AFM singularity in ρ(T) shifts to lower temperatures, as expected for antiferromagnets. In concert with the σ(H) data, the shift gets reversed in fields $\mu_0 H > 1$ T, and the anomaly rapidly broadens in strong magnetic fields (see Fig. 10). This behavior agrees with the occurrence of the metamagnetic transition near 0.8 T. It is worthwhile noting that even in a field of 9 T, the resistivity measured at 2 K is as large as 44 μΩcm. This finding supports the scenario of the structural disorder being responsible for the enhanced magnitude of the residual resistivity in the material investigated.

Fig. 11 presents the transverse magnetoresistance of $Ce_{3-x}RhGa_{10+3x}$ measured as a function of magnetic field applied perpendicular to the electric current. At 30 K, the magnetoresistance $\Delta\rho/\rho(H) = [\rho(H) -$

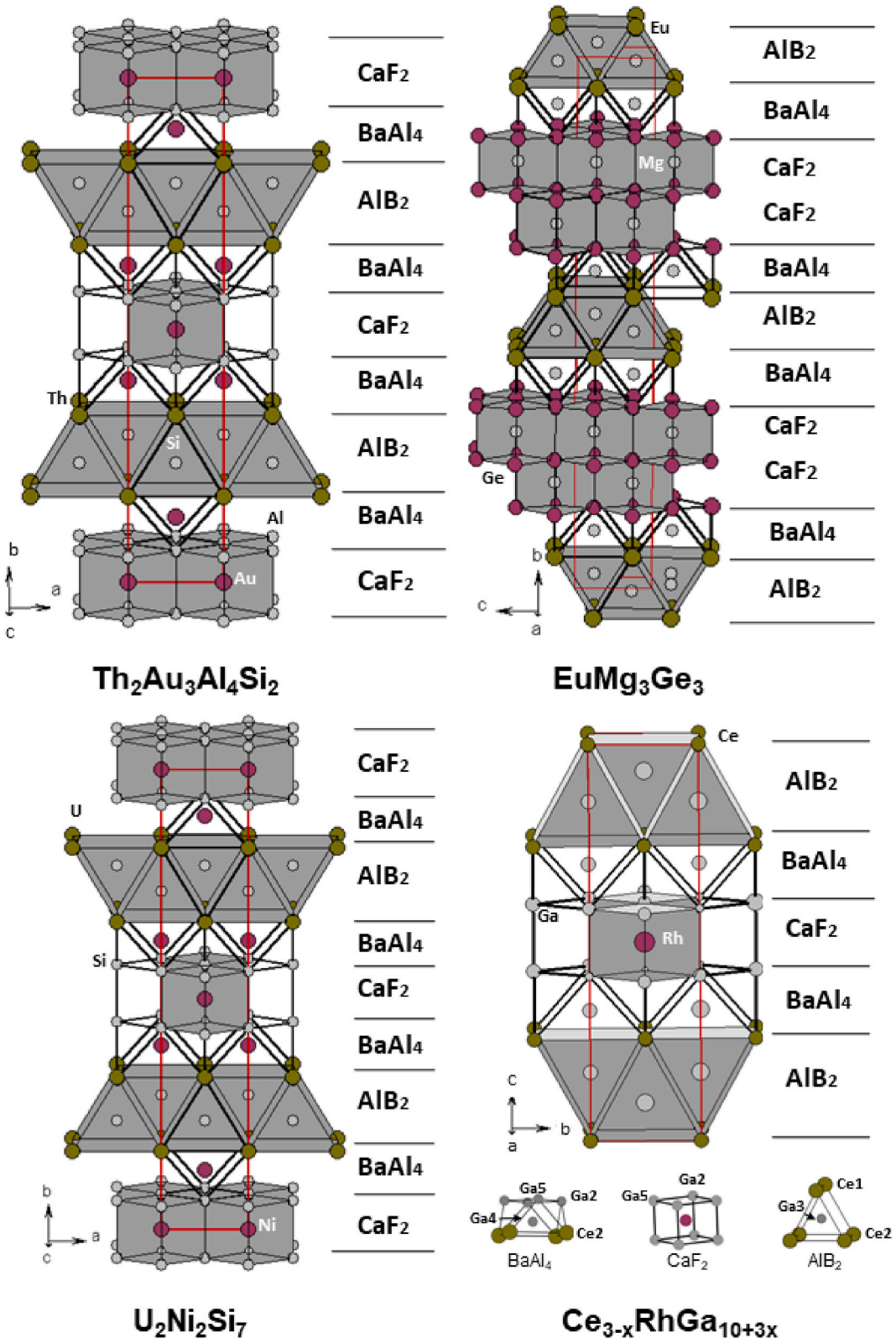

Fig. 5. $Th_2Au_3Al_4Si_2$, $U_2Ni_2Si_7$, $EuMg_3Ge_3$, and $Ce_{3-x}RhGa_{10+3x}$ structures in terms of linear intergrowth representation. Cell edges are outlined in red.

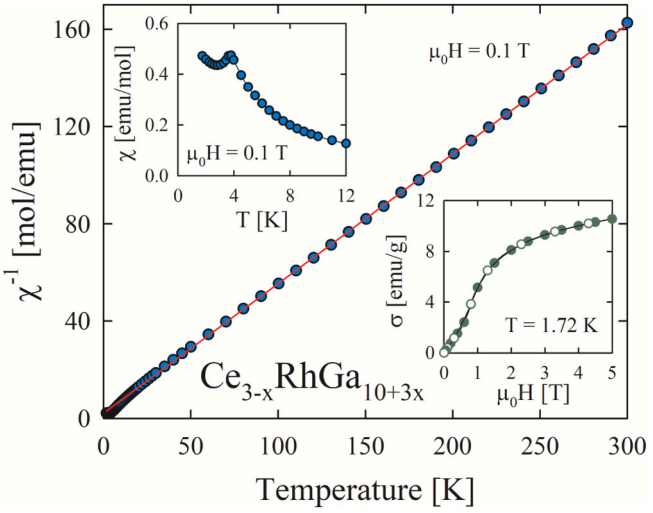

Fig. 6. Temperature dependence of the reciprocal magnetic susceptibility of $Ce_{3-x}RhGa_{10+3x}$ (x = 0.36) measured in a magnetic field of 0.1 T. The solid straight line represents the Curie-Weiss law. The upper inset shows the low-temperature magnetic susceptibility data. The lower inset displays the magnetic field variation of the magnetization in $Ce_{3-x}RhGa_{10+3x}$ (x = 0.36) taken at 1.72 K with increasing (full circles) and decreasing (open circles) magnetic field strength.

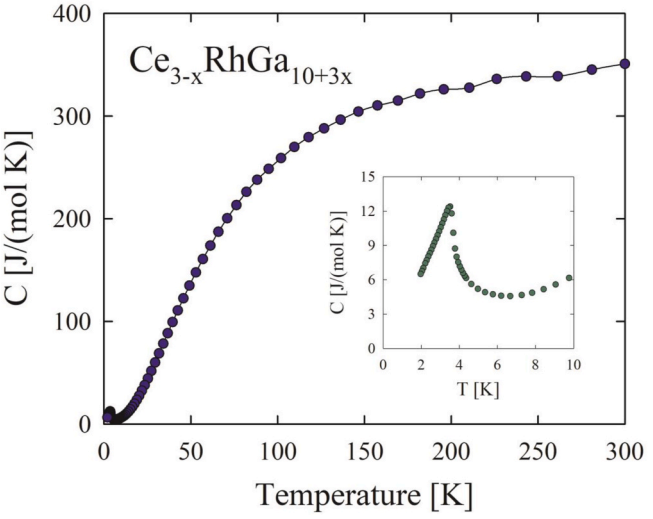

Fig. 7. Temperature dependence of the specific heat of $Ce_{3-x}RhGa_{10+3x}$ (x = 0.36). The inset shows the low-temperature data.

ρ(0)]/ρ(0) is slightly positive and can be attributed to Lorentz effect. With decreasing temperature, another contribution to Δρ/ρ becomes dominant, namely the Kondo effect that brings about a negative magnetoresistance with a characteristic parabolic-like magnetic field dependence. Below 10 K, the shape of Δρ/ρ(H) further changes, especially in strong magnetic fields. This behavior results from the AFM exchange interaction that gives positive contribution to the magnetoresistance. The largest magnitude of Δρ/ρ (for $\mu_0 H > 5$ T) was found at 4 K, i.e. just above T_N; the value measured in 9 T was about 10%. As can be inferred from Fig. 11, in the ordered state, scattering conduction electrons on the AFM magnons causes reduction in the absolute magnitude of the magnetoresistance and markedly influences the overall shape of the Δρ/ρ(H) isotherms.

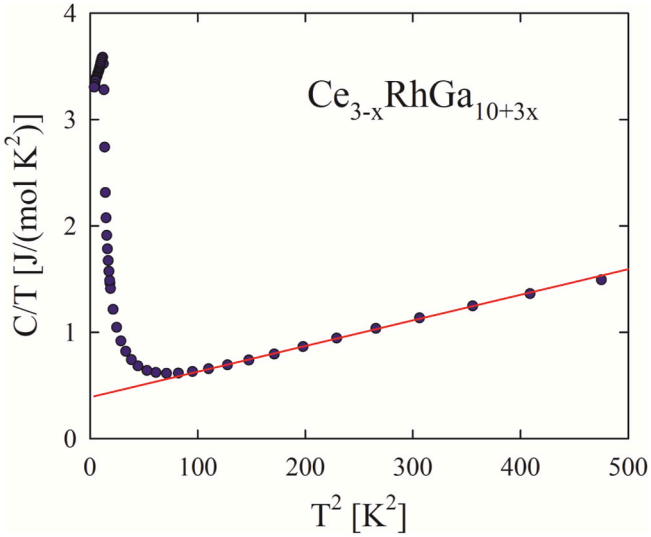

Fig. 8. The low-temperature specific heat data presented as specific heat over temperature versus squared temperature. The solid straight line represents the Debye fit.

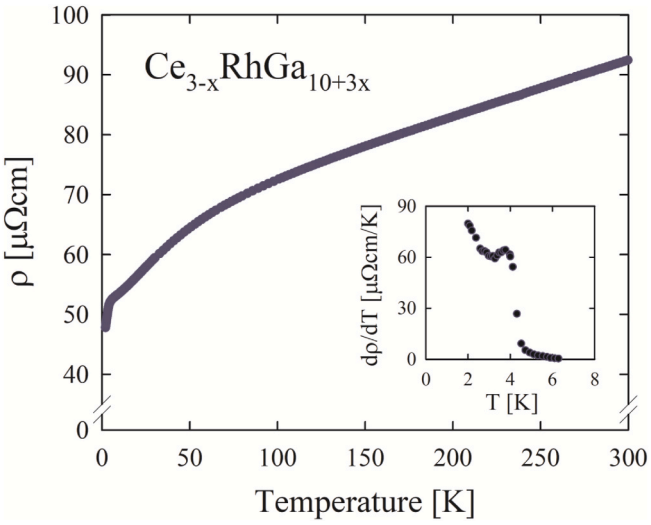

Fig. 9. Temperature dependence of the electrical resistivity of $Ce_{3-x}RhGa_{10+3x}$ (x = 0.36). The inset shows the low-temperature variation of the temperature derivative of the electrical resistivity.

4. . Conclusions

The novel cerium gallide $Ce_{3-x}RhGa_{10+3x}$ (x = 0.36) adopts a disordered modification of the Pr_3NiGa_{10} type structure with two additional Ga atom sites being partially occupied. One of the two Ce atom sites present in the crystallographic unit cell also shows partial occupancy. The crystal structure of $Ce_{3-x}RhGa_{10+3x}$ can be presented as stacking of blocks of the $BaAl_4$, CaF_2 and AlB_2 types.

The $Ce_{3-x}RhGa_{10+3x}$ (x = 0.36) compound exhibits Curie-Weiss paramagnetic behavior and antiferromagnetic ordering below T_N = 3.6 K. The novel gallide shows metallic-like electrical conductivity somewhat affected by the structural disorder. Its electrical transport is notably governed by scattering contributions due to crystalline electric field, Kondo and magnetic exchange interactions.

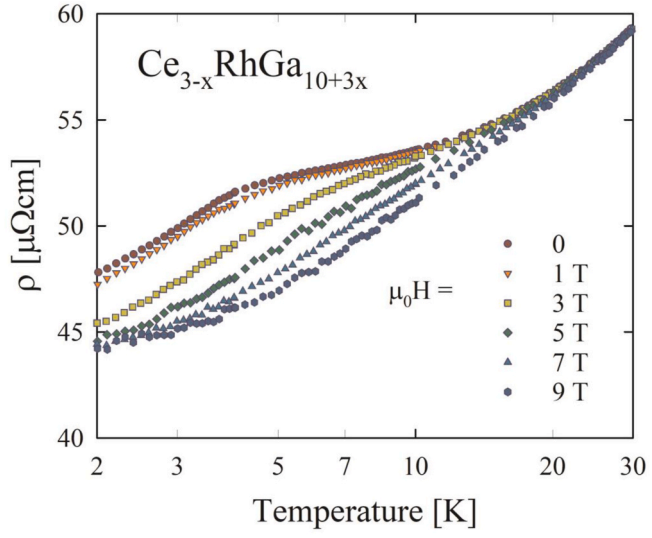

Fig. 10. The low-temperature electrical resistivity of $Ce_{3-x}RhGa_{10+3x}$ (x = 0.36) measured in several different magnetic fields applied perpendicular to electric current.

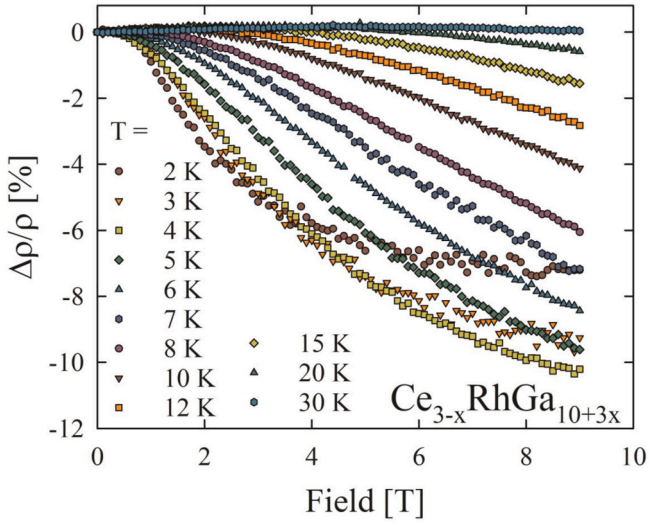

Fig. 11. Magnetic field dependencies of the transverse magnetoresistance of $Ce_{3-x}RhGa_{10+3x}$ (x = 0.36) measured at several different temperatures.

CRediT authorship contribution statement

Sergey Nesterenko: Formal analysis, Investigation, Writing - review & editing. **Anna Tursina:** Conceptualization, Formal analysis, Investigation, Writing - original draft. **Dariusz Kaczorowski:** Conceptualization, Investigation, Formal analysis, Supervision, Writing - original draft.

Declaration of Competing interest

The authors declare that they have no competing interest with the contents or subject of the manuscript.

Acknowledgements

This study was supported by the Russian Foundation for Basic Researches (Grant No 19-03-00135a). X-ray and EDX measurements were performed at User Facilities Center of Lomonosov Moscow State University under support of Ministry of Education and Science of Russia (Contract N 16.552.11.7081).

References

[1] A. Fedorchuk, Yu Grin, Crystal structure and chemical bonding in gallides of rare-earth metals, in: J.-C. Bunzli, V. Pecharsky (Eds.), Handbook on the Physics and Chemistry of Rare Earths, 53, Elsevier, North Holland, 2018, pp. 81–143. https://doi: 10.1016/bs.hpcre.2018.04.002.

[2] D. Joshi, Magnetic Behaviour in Rare Earth Intermetallic Indides and Gallides, LAP LAMBERT Acad. Publ., 2020.

[3] R.T. Macaluso, S. Nakatsuji, H. Lee, Z. Fisk, M. Moldovan, D.P. Young, J.Y. Chan, Synthesis, structure, and magnetism of a new heavy-fermion antiferromagnet, $CePdGa_6$, J. Solid State Chem. 174 (2003) 296–301. https://doi:10.1016/s0022-4596(03)00223-8.

[4] R.T. Macaluso, J.N. Millican, S. Nakatsuji, H.-O. Lee, B. Carter, N.O. Moreno, J. Y. Chan, A comparison of the structure and localized magnetism in Ce_2PdGa_{12} with the heavy fermion $CePdGa_6$, J. Solid State Chem. 178 (2005) 3547–3553. https://doi:10.1016/j.jssc.2005.09.013.

[5] J.N. Millican, R.T. Macaluso, D.P. Young, M. Moldovan, J.Y. Chan, Synthesis, structure, and physical properties of Ce_2PdGa_{10}, J. Solid State Chem. 177 (2004) 4695–4700. https://doi: 10.1016/j.jssc.2004.08.030.

[6] I. Das, E.V. Sampathkumaran, Ferromagnetism in the alloys $CeAg_{0.75}Ga_{3.25}$, $CePd_{0.3}Ga_{3.7}$, and $CeAg_{0.6}Al_{3.4}$, Phys. Rev. B 48 (1993) 16103, https://doi.org/10.1103/PhysRevB.48.16103.

[7] A.P. Pikul, D. Kaczorowski, P. Wiśniewski, Suppression of ferromagnetism in solid solution $CePd_xGa_{4-x}$, J. Alloys Compd. 648 (2015) 636–640. https://doi: 10.1016/j.jallcom.2015.07.007.

[8] J.W. Kim, Y.S. Kwon, Anomalous magnetic properties of heavy fermion $CePdGa_3$, Physica B 378–380 (2006) 833–834. https://doi:10.1016/j.physb.2006.01.306.

[9] R.T. Macaluso, M. Francisco, D.P. Young, S. Stadler, J.F. Mitchell, U. Geiser, M. Kanatzidis, Structure and properties of rhombohedral $CePd_3Ga_8$: a variant of the cubic parent compound with $BaHg_{11}$ structure type, J. Solid State Chem. 184 (2011) 3185–3189. https://doi: 10.1016/j.jssc.2011.10.001.

[10] A. Lacerda, P. Canfield, W. Beyermann, M. Hundley, J. Thompson, G. Sparn, J. Goldstone, Possible heavy-fermion behavior and field-induced transitions in new R-Pt-Ga compounds, J. Alloys Compd. 181 (1992) 191–196. https://doi:10.1016/0925-8388(92)90311-v.

[11] T. Yamashita, S. Ohara, Non-Fermi liquid behavior on heavy-fermion system $Ce_2Pt_6Ga_{15}$, J. Phys.: Conf. Ser 400 (2012), 042074. https://doi: 10.1088/1742-6596/400/4/042074.

[12] D. Gnida, D. Kaczorowski, Magnetism and weak electronic correlations in Ce_2PdGa_{12}, J. Phys. Condens. Matter 25 (2013) 145601. https://doi:10.1088/0953-8984/25/14/145601.

[13] S. Nallamuthu, T.P. Rashid, V. Krishnakumar, C. Besnard, H. Hagemann, M. Reiffers, R. Nagalakshmi, Anisotropic magnetic, transport and thermodynamic properties of novel tetragonal Ce_2RhGa_{12} compound, J. Alloys Compd. 604 (2014) 379–383. https://doi:10.1016/j.jallcom.2014.03.067.

[14] O. Sichevych, C. Krellner, Y. Prots, Y. Grin, F. Steglich, Physical properties and crystal chemistry of $Ce_2Ga_{12}Pt$, J. Phys. Condens. Matter 24 (2012) 256006. https://doi:10.1088/0953-8984/24/25/256006.

[15] Y.J. Zhang, B. Shen, F. Du, Y. Chen, J.Y. Liu, H. Lee, H.Q. Yuan, Structural and magnetic properties of antiferromagnetic Ce_2IrGa_{12}, Phys. Rev. B 101 (2020), 024421, https://doi.org/10.1103/physrevb.101.024421.

[16] J.L. Sarrao, L.A. Morales, J.D. Thompson, B.L. Scott, G.R. Stewart, F. Wastin, J. Rebizant, P. Boulet, E. Colineau, G.H. Lander, Plutonium-based superconductivity with a transition temperature above 18 K, Nature 420 (2002) 297–299, https://doi.org/10.1038/nature01212.

[17] W. Xie, H. Luo, B.F. Phelan, T. Klimczuk, F.A. Cevallos, R.J. Cava, Endohedral gallide cluster superconductors, Proc. Nat. Acad. Sci. USA 112 (2015) E7048–E7054. https://doi:10.1073/pnas.1522191112.

[18] A. Tursina, S. Nesterenko, V. Avzuragova, D. Kaczorowski, New Ternary Gallides, $CeRh_2Ga_2$ and $Ce_{3-x}RhGa_{10+x}$, 20th International Conference on Solid Compounds of Transition Elements, Book of abstracts, Zaragoza, Spain, 11-15 April 2016, p. 85.

[19] V.B. Zlokazov, V.V. Chernyshev, MRIA - a program for a full profile analysis of powder multiphase neutron-diffraction time-of-flight (direct and Fourier) spectra, J. Appl. Crystallogr. 25 (1992) 447–451. https://doi: 10.1107/S0021889891013122.

[20] G.M. Sheldrick, Crystal structure refinement with SHELXL, Acta Crystallogr. C. 71 (2015) 3–8, https://doi.org/10.1107/S2053229614024218.

[21] L.M. Gelato, E. Parthe, STRUCTURE TIDY–a computer program to standardize crystal structure data, J. Appl. Crystallogr. 20 (1987) 139–143. https://doi:10.1107/S0021889887086965.

[22] K. Brandenburg, DIAMOND. Release 3.2k, Crystal Impact Gmbh, Bonn, Germany, 2005.

[23] B. Buschinger, C. Geibel, M. Weiden, C. Dietrich, G. Cordier, G. Olesch, J. Köhler, F. Steglich, Crystallographic and physical properties of new ternary $R_2T_3X_9$ (R = La, Ce, U, T = Rh, Ir, X = Al, Ga) compounds, J. Alloys Compd. 260 (1997) 44–49. https://doi: 10.1016/S0925-8388(97)00174-6.

[24] Yu. Grin N., Ya. Yarmolyuk P., I.V. Rozhdestvenskaya, The crystal chemistry of a series of inhomogeneous linear structures. IV: the crystal structure of the compounds R_3NiGa_{10} (R = Ce, Pr, Nd), Kristallografiya 28 (1983) 806–808.

[25] F. Haarmann, Yu. Prots, S. Göbel, H.G. von Schnering, Crystal structure of tristrontium octagallide, $Sr_{3-x}Ga_{8+3x}$ (x = 0.15), Z. Kristallogr. NCS. 221 (2006) 257–258. https://doi: 10.1524/ncrs.2006.0063.

[26] O. Sichevych, Yu. Prots, Yu. Grin, Re-investigation of the crystal structure of trieuropium octagallide, $Eu_{3-x}Ga_{8+3x}$ (x = 0.12), Z. Kristallogr. NCS 221 (2006) 265–266, https://doi.org/10.1524/ncrs.2006.0067.
[27] Q. Lin, T. Mishra, J.D. Corbett, Hexagonal-diamond-like gold lattices, Ba and (Au, T)$_3$ interstitials, and delocalized bonding in a family of intermetallic phases $Ba_2Au_6(Au,T)_3$ (T = Zn, Cd, Ga, In, or Sn), J. Am. Chem. Soc. 135 (2013) 11023–11031. https://doi: 10.1021/ja401378q.
[28] B. Gerke, A. Korthaus, O. Niehaus, F. Haarmann, R. Pöttgen, Triangular Zn_3 and Ga_3 units in $Sr_2Au_6Zn_3$, $Eu_2Au_6Zn_3$, $Sr_2Au_6Ga_3$, and $Eu_2Au_6Ga_3$ – structure, magnetism, ^{151}Eu Mössbauer and ^{69,71}Ga solid state NMR spectroscopy, Z. Naturforsch. B Chem. Sci. 71 (2016) 567–577. https://doi: 10.1515/znb-2016-0033.
[29] P. Pyykkö, M. Atsumi, Molecular single-bond covalent radii for elements 1–118, Chem. Eur J. 15 (2009) 186–197. https://doi:10.1002/chem.200800987.
[30] J. Emsley, The Elements, Oxford University Press, New York, 1991.
[31] M. Pani, M.L. Fornasini, Examples of linear structures of intermetallic compounds described as intergrowths of segments of simple basic structures, Z. Kristallogr. 190 (1990) 127–133. https://doi:10.1524/zkri.1990.190.1-2.127.
[32] Yu. Grin N., in: E. Parthe (Ed.), The Intergrowth Concept as a Useful Tool to Interpret and Understand Complicated Intermetallic Structures, Modern Perspectives in Inorganic Chemistry, NATO ASI Series, Ser. C: Math. Phys. Sci., 382, Springer, Dordrecht, 1992, pp. 77–95.
[33] Y.N. Grin, Y.P. Yarmolyuk, E.I. Gladyshevskii, Crystal chemistry of series of inhomogeneous linear structures. 1. Symmetry and numerical symbols of structures composed of fragments of structural types $BaAl_4$, CaF_2, AlB_2, $AuCu_3$, Cu, α-Fe, and α -Po, Krystallografiya 27 (1982) 686–692.
[34] S.E. Latturner, D. Bilc, S.D. Mahanti, M.G. Kanatzidis, Quaternary intermetallics grown from molten aluminum. The homologous series $Th_2(Au_xSi_{1-x})[AuAl_2]_nSi_2$ (n = 1, 2, 4), Chem. Mater. 14 (2002) 1695–1705. https://doi:10.1021/cm010909w.
[35] L.G. Aksel'rud, Ya. Yarmolyuk P., E.I. Gladyshevskii, Crystal structure of the uranium nickel silicide compound $U_2Ni_2Si_7$, Dop. Akad. Nauk URSR, Ser. A. 7 (1975) 643–645.
[36] O.F. Zmii, E.I. Gladyshevskii, V.S. Bul'o, Crystal structure of the compound $EuMg_3Ge_3$, Kristallografiya 18 (1973) 277–280.